The Astrophysical Journal Letters, 846:L1 (7pp), 2017 September 1 https://doi.org/10.3847/2041-8213/aa85dd

NGC 1866: First Spectroscopic Detection of Fast-rotating Stars in a Young LMC Cluster

A. K. Dupree[1], A. Dotter[1], C. I. Johnson[1], A. F. Marino[2], A. P. Milone[2], J. I. Bailey, III[3], J. D. Crane[4], M. Mateo[5], and E. W. Olszewski[6]
[1] Harvard-Smithsonian Center for Astrophysics, 60 Garden Street, Cambridge, MA 02138, USA
[2] Australian National University, The Research School of Astronomy and Astrophysics, Mount Stromlo Observatory, Weston Creek, ACT 2611, Australia
[3] Leiden Observatory, Niels Bohrweg 2, NL-2333 CA Leiden, The Netherlands
[4] The Observatories of the Carnegie Institution for Science, 813 Santa Barbara Street, Pasadena, CA 91101, USA
[5] Department of Astronomy, University of Michigan, Ann Arbor, MI 48109, USA
[6] The University of Arizona, 933 N. Cherry Avenue, Tucson, AZ 85721, USA
Received 2017 June 8; revised 2017 August 9; accepted 2017 August 10; published 2017 August 23

Abstract

High-resolution spectroscopic observations were taken of 29 extended main-sequence turnoff (eMSTO) stars in the young (~200 Myr) Large Magellanic Cloud (LMC) cluster, NGC 1866, using the Michigan/*Magellan* Fiber System and MSpec spectrograph on the *Magellan*-Clay 6.5 m telescope. These spectra reveal the first direct detection of rapidly rotating stars whose presence has only been inferred from photometric studies. The eMSTO stars exhibit Hα emission (indicative of Be-star decretion disks), others have shallow broad Hα absorption (consistent with rotation $\gtrsim$150 km s^{-1}), or deep Hα core absorption signaling lower rotation velocities ($\lesssim$150 km s^{-1}). The spectra appear consistent with two populations of stars—one rapidly rotating, and the other, younger and slowly rotating.

Key words: globular clusters: individual (NGC 1866) – stars: emission-line, Be – stars: rotation – techniques: spectroscopic

1. Introduction

Identification of multiple main sequences in old Milky Way globular clusters from *Hubble Space Telescope* (*HST*) photometry (Bedin et al. 2004; Piotto et al. 2007; Gratton et al. 2012) created a fundamental change in our concept of their stellar populations for it suggested that cluster stars are neither coeval nor chemically homogeneous. This paradigm shift results from the fact that multiple sequences are visible along the entire color–magnitude diagram (CMD) signaling two or more generations of stars.

No completely successful scenario exists to explain multiple populations, although many possibilities have been offered. The most popular suggests that a second generation of enriched (polluted) stars forms from gas that was processed at high temperatures in the cores and/or envelopes of intermediate- to high-mass first-generation stars. Each of the many possibilities appears to have at least one fatal flaw (Bastian et al. 2015; Renzini et al. 2015; Charbonnel 2016). The situation becomes more complicated when investigating younger clusters, which could reveal the predecessors of the Milky Way clusters.

Photometric studies of young and intermediate-age clusters (age <2 Gyr) in the Large Magellanic Cloud (LMC) support yet another scenario. They have revealed an extended (broadened) main-sequence turnoff (eMSTO) and/or a bimodal main sequence (Mackey et al. 2008; Milone et al. 2009; Goudfrooij et al. 2009, 2014). This discovery could imply that a prolonged (100–500 Myr) star formation history occurred (Mackey et al. 2008; Conroy & Spergel 2011; Keller et al. 2011). This could be an attractive simple explanation as there are concerns about the lack of active star formation in clusters older than 10 Myr (Niederhofer et al. 2016) and the absence of natal cluster gas after 4 Myr (Hollyhead et al. 2015) suggesting that multiple stellar generations may not be present.

Photometry of young (~300 Myr) stellar clusters also reveals the eMSTO and a bifurcated main sequence (D'Antona et al. 2015; Milone et al. 2016, 2017). A recent claim of detection of young stellar objects in some young clusters in the LMC hints at ongoing star formation (For & Bekki 2017). However, other scenarios have been introduced to explain the eMSTO and bifurcated main sequence including a range of ages (Mackey & Broby Nielsen 2007; Milone et al. 2009; Keller et al. 2011; Correnti et al. 2014; Goudfrooij et al. 2014), different rotation rates (Bastian & deMink 2009; D'Antona et al. 2015; Niederhofer et al. 2015; Bastian et al. 2016; Milone et al. 2016, 2017), braking of rapid rotators (D'Antona et al. 2017), or different metallicities (Milone et al. 2015).

Our target, NGC 1866, a 200 Myr cluster in the LMC, displays the eMSTO and also a bifurcated main sequence (Milone et al. 2017). These characteristics are not due to photometric errors, field-star contamination, differential reddening, or non-interacting binaries (Milone et al. 2016, 2017). Comparison with isochrones (Milone et al. 2017) suggests that the best-fit of the bifurcated main sequence comes from rotating stellar models for the red main sequence and non-rotating models for the blue main sequence. It is believed that abundances are similar among the populations of NGC 1866 (Mucciarelli et al. 2011), although the ages are not, and may range from 140 to 220 Myr (Milone et al. 2017). Isochrone modeling provides good agreement with the main-sequence objects, but the fit to the eMSTO objects is not as satisfactory. Variable stars, such as δ Scuti objects, might also produce an extended turnoff (Salinas et al. 2016); however, these stars become significant in older clusters (1–3 Gyr) where the turnoff from the main sequence coincides with the instability strip. Stellar rotation not only affects the colors of the stars but also their lifetimes through rotational mixing. Rotation could possibly cause the observed spreads in the CMD (Bastian & deMink 2009). In fact, narrowband and broadband photometry of bright stars in two young LMC clusters hint at the appearance of Hα emission (Bastian et al. 2017), which is

interpreted as signaling the presence of rapidly rotating Be stars.

No direct measure of rotation has been carried out for individual stars populating the eMSTO in LMC clusters. In this Letter, we report the first high-resolution spectroscopy of the Hα line in 29 stars in the extended turnoff region of the LMC cluster NGC 1866. Synthesis of model spectra indicated that narrow photospheric features would be "washed out" and too subtle to detect if the stars are rapidly rotating, making the Hα transition a feature of choice to characterize the rotational state of the star.

2. Spectroscopic Material

Stellar spectra were obtained with the Michigan/*Magellan* Fiber System (M2FS; Mateo et al. 2012) and the MSpec multi-object spectrograph mounted on the *Magellan*-Clay 6.5 m telescope at Las Campanas Observatory. The fibers have a diameter of 1.″2 and can span a field of view nearly 30 arcmin in diameter. A 180 μm slit yielded a resolving power $\lambda/\Delta\lambda \sim$ 28,000. The spectra were binned by 2 pixels in the spatial direction and remained at 1 pixel along the dispersion.

The selected targets, which are likely members of the cluster NGC 1866, were identified by Milone et al. (2017) from the Ultraviolet and Visual Channel of the Wide Field Camera 3 (UVIS/WFC3) of the *HST*. Images taken with the F336W filter and the F814W filter provided the photometry and astrometry. Milone et al. (2017) noted that the apparent stellar density became constant at radial distances greater than about 3 arcmin from the cluster center and concluded that cluster members did not extend beyond that distance. Our targets comply with this criterion. In addition, we selected targets separated by 2.5 arcsec at a minimum from any neighboring stars that are brighter and located away from stars less than 2 mag fainter in the F814W band than the target star. With this selection criterion, coupled with the requirements on fiber placement, very few stars remain within the half-light radius of the cluster (41 arcsec); in fact only two of our targets are located there. The vast majority lie between 41 arcsec and ~180 arcsec from the center. This criterion identified ~150 acceptable targets, spanning $V = 16.2$–20. Positions of the guide and acquisition stars were verified by comparison with the 2MASS catalog and WFI images. The software code for M2FS fiber positioning selected targets according to our priorities.

We chose the filter "Bulge-GC1," which spans 6120–6720 Å over 6 echelle orders and allows up to 48 fibers to be placed on our targets. In practice, several fibers are placed on the sky; thus, we obtained about 43 stellar targets per configuration. Some targets were "lost" due to low fiber sensitivity, neighboring very bright stars, or possibly inaccurate coordinates. Two configurations—a bright and faint selection—each spanning about 2 mag were implemented. Our principal configuration was observed on 2016 December 8 and 12 with seven exposures totaling 5.5 hr varying between 2100 s and 2700 s each. A fainter target configuration was observed on 2016 December 11 and 13, but the spectra were severely compromised by the full moon.

Standard IRAF procedures performed the bias subtraction, overscan trimming, and combination of the four individual CCD quadrants into one monolithic array. The *dohydra* task was implemented for aperture identification and tracing, scattered-light subtraction, flat-fielding, and line identification for wavelength calibration from the ThAr comparison lamp. Sky emission lines were identified and removed individually, and the Hα order was continuum normalized with a cubic spline, omitting the Hα region. A detailed description of the procedures can be found in Johnson et al. (2015).[7] We obtained Hα spectra for 29 targets within a 3 arcmin radius of the cluster center. Comparison of stars in the reference field within the color and magnitude boundaries of our sample suggests that 10% of our targets (comprising three targets) in the cluster field might not be cluster members. The solar Hα line in absorption frequently appears in the spectra at shorter wavelengths than the LMC spectral features but nevertheless allows definition of the continuum on the short-wavelength side of Hα. Target stars, their positions, magnitudes, and Hα characteristics are given in Table 1.

3. Analysis

Hα spectra of the 29 targets located within 3 arcmin of the cluster center are shown in Figure 1 where both emission and absorption can be found. The emission features are centered on the velocity of the cluster, $+298.5\,\mathrm{km\,s^{-1}}$ (Mucciarelli et al. 2011). The profiles are typical of those found in Be stars in which the emission arises in a Keplerian decretion disk surrounding a rapidly rotating star (Reid & Parker 2012; Rivinius et al. 2013; Paul et al. 2017). Differences in the profile shapes result from the angle of observation, from pole-on to equator (Struve 1931). In particular, the narrow "wine-bottle" Hα profile of Object 58 suggests it is viewed nearly pole-on; many others (Objects 14, 26, 56, 62, and 89) exhibit a deep central absorption thought to arise from absorption in the cool circumstellar disk when viewed edge-on (Hummel 1994). The line widths at the continuum level vary as well, from $\pm$ $110\,\mathrm{km\,s^{-1}}$ in the pole-on object to $>\pm 200\,\mathrm{km\,s^{-1}}$ in stars observed at intermediate angles.

Absorption profiles shown in Figure 1 are shallow and broad for many stars. Hα absorption wings in B stars are indicative of the stellar gravity, and the core of the line responds to rotation, becoming more shallow with increasing values of $v \sin i$. Several of the stars can be seen by visual inspection to have a deep (narrow) core in the absorption profile.

We further examine the absorption profiles in two ways: profile synthesis and broadening assessment. In the first instance, theoretical Hα absorption profiles are compared to the observed profiles for three bright targets in Figures 2(a)–(c). Hα profiles from Castelli and Kurucz LTE models[8] were broadened using a Gaussian convolution and overlaid on the profiles; also shown are reasonable excursions to the profile with higher and lower rotational velocities. Comparison of LTE versus non-LTE calculations of Hα profiles shows that LTE profiles are adequate for stars cooler than ~22,000 K (Przybilla & Butler 2004; Nieva & Przybilla 2007). *HST* colors predicted from the Choi et al. (2016) models suggest these targets have $T_{\rm eff} \sim$ 15,000 K. Synthesis of the spectra for Objects 10 and 12 suggests $v \sin i \sim 70$–$100\,\mathrm{km\,s^{-1}}$ in contrast to a value $\sim 200\,\mathrm{km\,s^{-1}}$ for Object 30. These values provide a lower limit to the true velocity because the orientations of the stars are unknown. Second, we developed a broadening parameter defined as the ratio of the central depth to the line profile depth at a wavelength 4 Å longward of line

[7] An outline of procedures is available online (https://www.cfa.harvard.edu/oir/m2fsreduction.pdf).

[8] Available at http://kurucz.harvard.edu.

Table 1
NGC 1866 Targets

Object	R.A. (2000.0)	Decl. (2000.0)	m_{F336W}	B	V	m_{F814W}	Color[a]	d (arcmin)[b]	R_{c+4}[c]	Key[d]
1[e]	78.374466	−65.481554	18.048	18.670	18.468	18.506	−0.458	1.39	...	1
3	78.431151	−65.470138	15.661	16.732	16.843	16.753	−1.092	0.58	...	1
10	78.418615	−65.475645	16.548	16.937	17.019	17.022	−0.474	0.69	0.79	2
12	78.470013	−65.419725	16.428	16.881	17.038	17.095	−0.667	3.05	0.75	2
14	78.425251	−65.454748	16.887	22.488	15.825	17.177	−0.290	0.67	...	1
15	78.369840	−65.465653	16.907	17.159	17.150	17.199	−0.292	1.06	...	1
17[f]	78.477155	−65.468106	18.134	18.679	18.723	18.705	−0.571	1.64	0.87	2
26	78.393400	−65.455855	17.140	17.290	17.166	17.390	−0.250	0.69	...	1
30	78.360408	−65.473644	17.046	17.423	17.437	17.493	−0.447	1.40	0.93	2
31	78.447226	−65.477066	17.114	17.551	17.493	17.525	−0.411	1.16	0.73	2
36	78.449744	−65.441929	16.707	17.687	17.569	17.677	−0.970	1.65	0.74	2
40	78.366140	−65.457688	17.164	17.633	17.639	17.727	−0.563	1.21	0.64	2
48	78.459678	−65.436704	17.454	17.811	17.795	17.816	−0.362	2.04	0.93	2
56	78.409850	−65.475827	17.619	18.004	18.024	17.955	−0.336	0.69	...	1
58	78.378488	−65.482908	17.389	17.864	17.910	17.968	−0.579	1.39	...	1
61	78.354382	−65.457718	17.460	17.931	17.925	17.983	−0.523	1.49	0.76	2
62	78.424431	−65.442766	17.940	18.034	17.995	17.991	−0.051	1.34	...	1
63	78.479936	−65.458286	17.272	17.911	17.987	18.010	−0.738	1.73	0.77	2
65	78.398687	−65.476448	17.539	17.927	17.932	18.037	−0.498	0.79	...	1
67	78.441385	−65.452302	17.603	18.019	18.084	18.052	−0.449	1.03	...	1
69	78.495511	−65.440840	17.503	18.006	18.030	18.096	−0.593	2.52	0.93	2
71	78.463359	−65.451612	17.460	18.023	18.105	18.130	−0.670	1.49	0.84	2
78	78.457044	−65.466589	17.766	18.247	18.224	18.263	−0.497	1.13	0.95	2
79	78.473464	−65.449753	18.127	18.306	18.314	18.290	−0.163	1.77	0.84	2
83	78.441541	−65.440489	18.002	18.392	18.355	18.367	−0.365	1.61	...	1
86	78.510130	−65.437927	17.809	18.222	18.240	18.421	−0.612	2.92	0.95	2
88	78.395433	−65.444091	18.291	18.899	18.898	18.428	−0.137	1.29	0.80	2
89	78.452582	−65.456036	18.269	18.559	18.491	18.432	−0.163	1.13	...	1
91	78.443073	−65.430659	17.848	18.405	18.388	18.460	−0.612	2.17	0.80	2

Notes.
[a] Color defined by $m_{F336W} - m_{F814W}$.
[b] Cluster center at R.A. (J2000): 05:13:38.92; decl. (J2000): −65:27:52.75 (McLaughlin & van der Marel 2005).
[c] Ratio of depth of Hα line core to depth at +4 Å in absorption line profiles.
[d] 1: Hα emission; 2: Hα absorption.
[e] Spectrum from a second M2FS configuration: 2016 December 13 (UT), total exposure 4.5 hr.
[f] Spectrum from a second M2FS configuration: 2016 December 11 (UT), total exposure 3 hr.

center: R_{c+4}. This ratio was measured for the target stars after subtracting the solar scattered continuum. Model profiles demonstrate that this ratio increases with increasing velocity (Figure 2(d)). The dependence of the ratio on velocity appears similar for different values of the gravity. The observed profiles map velocities, v, from 50 to 250 km s^{-1}. Inspection of the Hα absorption profiles suggests that the majority of the targets with $v \lesssim 150$ km s^{-1} exhibit deep absorption cores; therefore, we denote these stars as "slow rotators" and label the stars with $v \gtrsim 150$ km s^{-1} as "fast rotators."

Theoretical critical velocities are shown in the *HST* CMD from MIST isochrones (Choi et al. 2016; Dotter 2016) for a range of ages corresponding to NGC 1866 (Figure 3). The isochrones have been shifted by the assumed distance and reddening of NGC 1866 ($(m - M)_0 = 18.31$, $E(B - V) = 0.11$; Milone et al. 2017). The MIST isochrones include the effects of rotation; those shown in Figure 3 are initialized with $\Omega/\Omega_{crit} = 0.4$ at the zero-age main sequence (ZAMS). The critical velocities for these targets (350–400 km s^{-1}) are larger than the values inferred from Figure 2(d). This may account for the lack of emission in Hα as stars have not achieved velocities necessary to shed material producing emission from a surrounding disk.

4. Discussion

The majority of eMSTO target stars fall into two categories: fast and slow rotators. Detection of Hα emission clearly signals a fast-rotating star with a Keplerian decretion disk—the Be phenomenon (Rivinius et al. 2013). We do not yet have measurements of the rotational velocity of the emission objects. The Hα absorption profiles indicate both rapidly and slowly rotating stars. Isochrone fitting to *HST* cluster photometry (Milone et al. 2017) suggested that the blue stars on the bifurcated main sequence are slowly rotating and represent two stellar generations of 140 and 220 Myr. Red main sequence stars are believed to be rapidly rotating ($\Omega = 0.9\Omega_{crit}$, a high fraction of the critical rotation rate, Ω_{crit}) and are consistent with an age of 200 Myr. Thus, our spectroscopic results confirm the conclusion of Milone et al. (2017) from photometry that identified fast and slowly rotating populations.

Figure 4 shows the *HST* CMD of NGC 1866 marked with targets and their characteristics. Inspection suggests that two targets, Objects 3 and 36, are outliers, and perhaps not cluster members because their colors are $\lesssim -1$ and cluster isochrones (Figure 3) do not extend to those colors. We exclude them from the calculation of median parameters. Taking the "narrow" absorption targets as those with $R_{c+4} \leqslant 0.90$, corresponding to

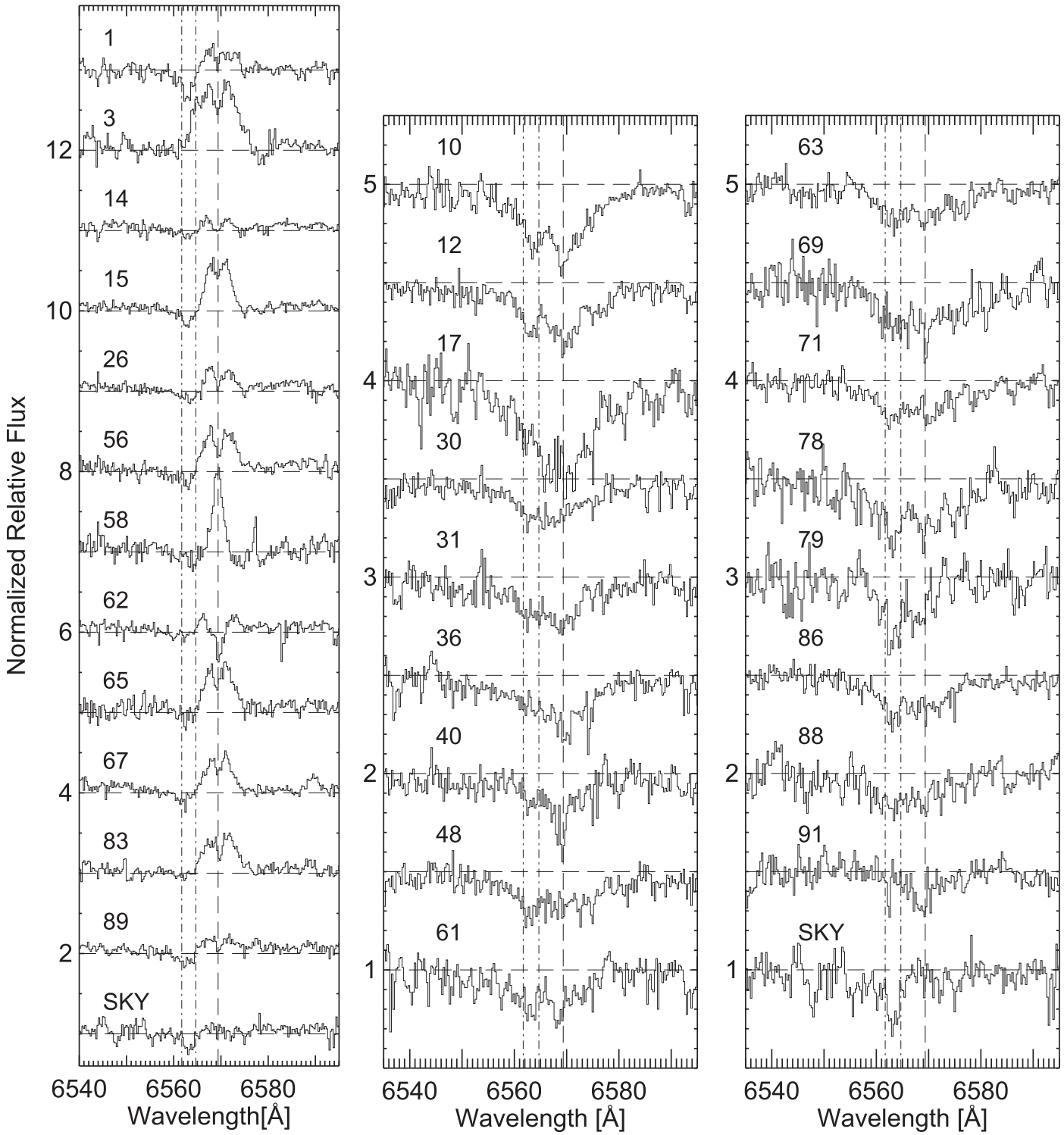

Figure 1. Hα region of the eMSTO stars in NGC 1866. Continuum-normalized spectra are binned to a resolution element and offset. The heliocentric velocity of the cluster, $+298.5 \pm 0.4$ km s^{-1} (Mucciarelli et al. 2011) is indicated by the broken line. The dotted–dashed lines mark the position of the scattered solar Hα line. A deep sky spectrum is shown. Object numbers are marked. Left panel: Hα emission objects. Center and right panels: stars exhibiting Hα absorption.

$v \lesssim 150$ km s^{-1}, in comparison to the targets with emission, we find that the median magnitudes, m_{F814W}, are essentially identical: 18.01 ± 0.418 (narrow) and 17.99 ± 0.377 (emission). Here, the dispersion is calculated as the median of the absolute deviations of magnitude about the median magnitude. However, the median colors suggest what is evident from Figure 4, namely, $m_{F336W} - m_{F814W}$ equals -0.56 ± 0.10 (narrow) and -0.34 ± 0.12 (emission). Targets exhibiting broad absorption $R_{c+4} > 0.90$ have a median magnitude similar to the others and a median color lying between the values of the other groups: -0.50 ± 0.10.

Additional characteristics of the stars can be compared to the results of the photometric studies of the cluster. Three results derive from the photometry:

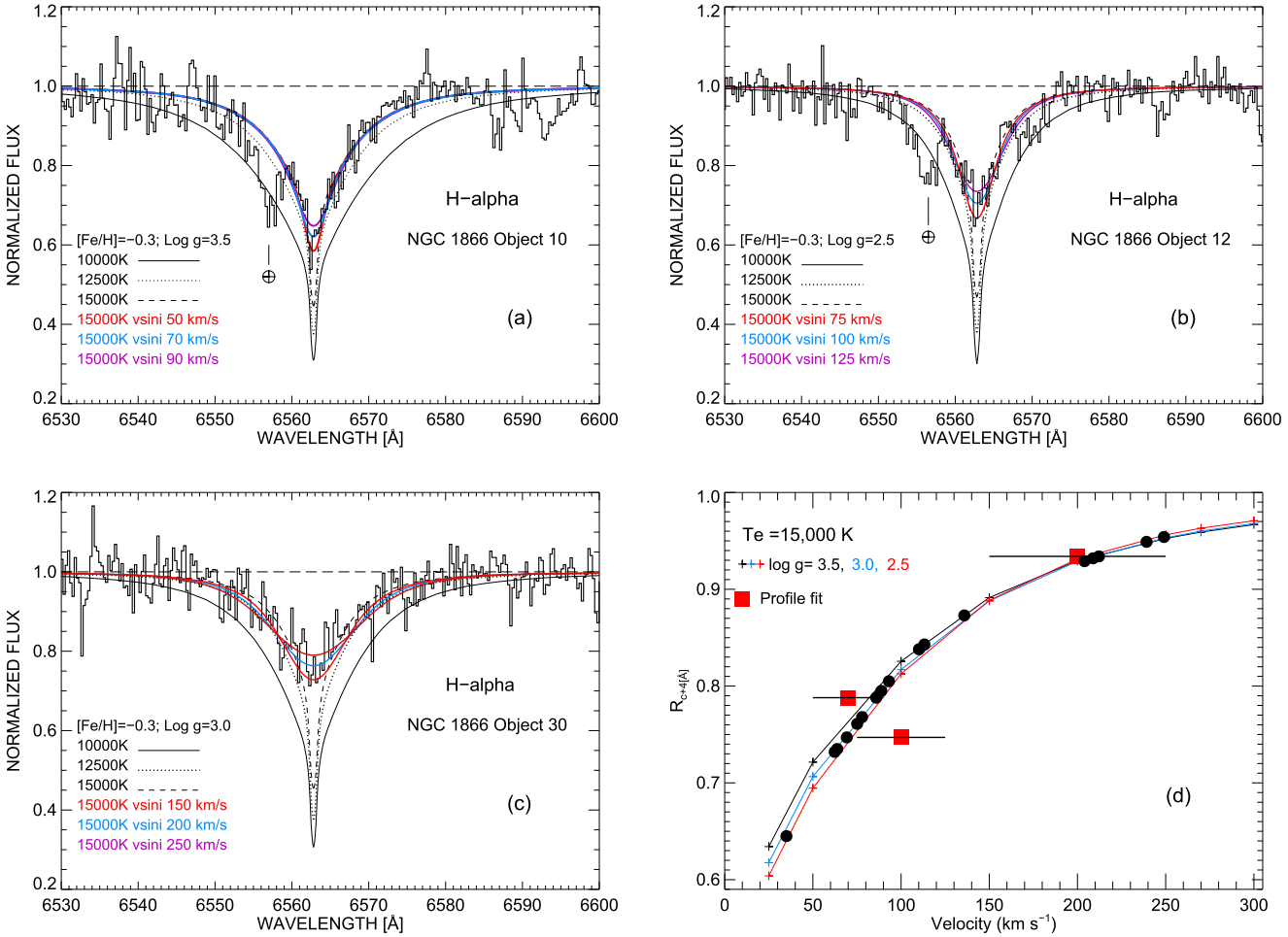

Figure 2. Panels (a)–(c): the Hα region in three objects exhibiting absorption. The spectra are centered on Hα. Hα sky contamination is marked in Objects 10 and 12. Theoretical profiles are from http://kurucz.harvard.edu for [Fe/H] = −0.3, log g values of 2.5–3.5, and broadened by a Gaussian to simulate rotation. The profiles suggest values of $v \sin i$ in excess of 50 km s^{-1} and ranging to ∼250 km s^{-1}. Approximate upper and lower limits of velocities are shown. Objects 10 and 12, exhibiting deep narrow Hα, are considered to be slow rotators as compared to Object 30. Panel (d): models of the relative central depth of Hα (R_{c+4}) as compared to model fits in panels (a)–(c) are denoted by red squares. The measured values of R_{c+4} for the targets are marked by black circles.

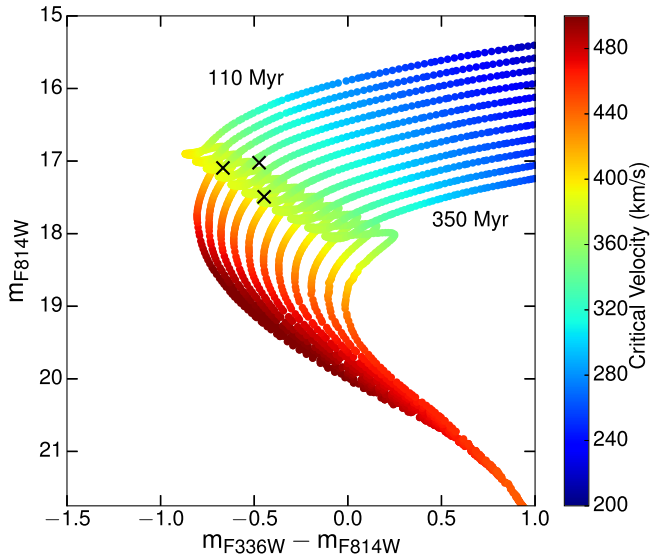

Figure 3. Expected breakup rotational velocities for ages spanning 110–350 Myr. Positions of the three stars from Figure 2 (Objects 10, 12, and 30) are marked and span isochrones from 140 to 225 Myr.

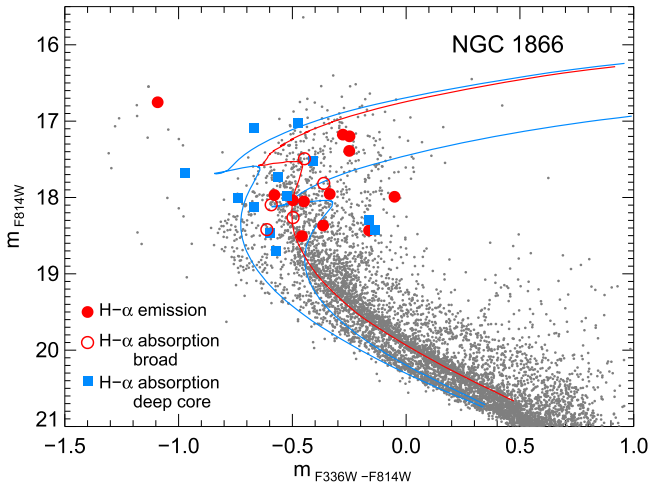

Figure 4. Characteristics of Hα profiles in NGC 1866 detected in the targets and displayed in the *HST* CMD. Isochrones are taken from Georgy et al. (2013) for non-rotating models ($\Omega = 0$) and ages of 140 Myr and 220 Myr (blue curves) and a rotating model ($\Omega = 0.9\Omega_{\rm crit}$) with an age of 200 Myr (red curve) similar to those shown by Milone et al. (2017). Stars within 3 arcmin from cluster center are marked by gray dots.

(1) *The red main sequence (rapid rotators) is more centrally concentrated than the blue main sequence (slow rotators).* Milone et al. (2017) find that the fraction of red main sequence stars within 1 arcmin of the cluster core is ∼0.68. Excluding outliers, the five targets within 1 arcmin include four stars that are fast rotators, exhibiting Hα emission (corresponding to a fraction of 0.80 ± 0.53 using Poisson statistics). Thus, there appears to be a preponderance of rapidly rotating stars in eMSTO objects located in the core of the cluster. Between 1 and 3 arcmin from the cluster center, our sample of 22 eMSTO stars indicates that the fast rotators decrease slightly to 0.55 ± 0.20 of the targets at this distance—although within the error estimate, the fraction remains comparable to that in the core.

(2) *The "blue component" comprises about 0.15 of the stars at the top of the main sequence.* We find the fraction of slow rotators (the blue component) to be 0.41 in the total eMSTO sample—a value higher than the photometric results.

(3) *Isochrone fitting suggests that the fast-rotating population has a velocity of 0.9 of critical velocity and corresponds to ∼200 Myr; the non-rotating isochrones indicate that the blue main sequence may harbor two populations of 140 and 220 Myr.* We find the rapid rotators occur to the red of the slowly rotating stars in the *HST* CMD (Figure 4). Inspection of isochrones (Milone et al. 2017) shown in Figure 4 suggests that the slowly rotating objects span the non-rotating isochrones between 140 Myr and slightly less than ∼220 Myr. The rotating population lies to the "red" of the slower-rotating stars, which suggests a population older than 200 Myr if $\Omega \sim 0.9\Omega_{\rm crit}$ and perhaps comparable to the slowly rotating objects. If so, this would remove the uncomfortable problem presented from photometry (Milone et al. 2017) of three populations harboring slow, fast, and slowly rotating stars formed in sequence.

Stars exhibiting Hα emission comprise a fraction of 0.41 of our total sample. This value is comparable to the fraction (Bastian et al. 2017) inferred from narrowband and broadband photometry of the eMSTO spanning 0.4–0.62 in the young LMC clusters NGC 1850 (79 Myr) and 0.33 in NGC 1856 (300 Myr). Photometric studies, however, give a lower limit to the emission fraction as only stars with strong emission are detected. Moreover, radial velocity shifts of LMC clusters can be significant and can compromise the detection of Hα in the narrow *HST* filter F656N frequently used as an Hα diagnostic. Spectroscopy is advantageous for Hα detection because weak emitters can be identified, rapid rotators without Hα emission can be detected, and radial velocity shifts are of no consequence. Inclusion of stars with broad Hα absorption raises the rapid rotation fraction to 0.61 among the eMSTO population in our total sample and implies the fraction must be higher in other clusters, e.g., NGC 1850 and NGC 1856, as well.

Direct spectroscopic measures of the eMSTO stars clearly demonstrates the presence of rapidly rotating stars that are cooler than a population of slowly rotating objects. It is not understood how such conditions were established. If the populations were coeval, slowly rotating stars evolve faster than the rapid rotators and they should have a lower turnoff luminosity. The CMD of the eMSTO objects (Figure 4) displays the opposite behavior that argues for an actual spread in age: the rapidly rotating population marks the (older) initial burst of star formation, followed by a second generation that is more slowly rotating. Isochrones in Figure 4 demonstrate that the younger non-rotating objects (at 140 Myr) lie to the "blue" of an older (200 Myr) isochrone that has a rotation close to the critical velocity; here, $\Omega = 0.9\Omega_{\rm crit}$. Recently, D'Antona et al. (2017) have speculated that rotational braking might mimic an age spread, a conjecture that requires spectroscopic confirmation by abundance measures or detection of a stellar wind. The spatial distribution is also puzzling. Goudfrooij et al. (2011) find that the upper eMSTO (presumably younger objects) is significantly more centrally concentrated than the lower eMSTO in many massive intermediate-age clusters in the LMC. This is in harmony with a second generation of stars formed from material shed by stars of the first generation. Our results might suggest a different scenario. It is the cooler eMSTO objects, spectroscopically determined to be fast rotators, that dominate within 1 arcmin of the cluster core, although we have a small sample. Perhaps this is typical of less massive and/or younger clusters. Yet, it is puzzling that the rapidly rotating stars are concentrated toward the cluster center (Milone et al. 2017) where it might be expected that a second stellar generation would form from the material of the first generation. This would appear to suggest that another scenario must be sought for young clusters.

We thank the anonymous referee for thoughtful comments and advice on the manuscript. A.F.M. and A.P.M. acknowledge support by the Australian Research Council through Discovery Early Career Researcher Awards DE160100851 and DE150101816. E.W.O. was partially supported by NSF grant AST1313006. This research has made use of NASA's Astrophysics Data System Bibliographic Services. And we have used data products from 2MASS, which is a joint project of the University of Massachusetts and IPAC/Caltech, funded by NASA and the NSF.

Facility: Magellan: Clay (M2FS).

ORCID iDs

A. K. Dupree https://orcid.org/0000-0002-8985-8489
A. Dotter https://orcid.org/0000-0002-4442-5700
C. I. Johnson https://orcid.org/0000-0002-8878-3315
J. D. Crane https://orcid.org/0000-0002-5226-787X

References

Bastian, N., Cabrera-Ziri, I., Niederhofer, F., et al. 2017, MNRAS, 465, 4795
Bastian, N., Cabrera-Ziri, I., & Salaris, M. 2015, MNRAS, 449, 3333
Bastian, N., & deMink, S. E. 2009, MNRAS, 398, L11
Bastian, N., Niederhofer, F., Kozhurina-Platais, V., et al. 2016, MNRAS, 460, L20
Bedin, L. R., Piotto, G., Anderson, J., et al. 2004, ApJL, 605, L125
Charbonnel, C. 2016, in EAS Publ. Ser. 80, Stellar Clusters: Benchmarks of Stellar Physics and Galactic Evolution, ed. E. Moraux, Y. Lebreton, & C. Charbonnel (Les Ulis: EDP Sciences), 177
Choi, J., Dotter, A., Conroy, C., et al. 2016, ApJ, 823, 102
Conroy, C., & Spergel, D. N. 2011, ApJ, 726, 36
Correnti, M., Goudfrooij, P., Kalirai, J. S., et al. 2014, ApJ, 793, 121
D'Antona, F., DiCriscienzo, M., Decressin, T., et al. 2015, MNRAS, 453, 2637
D'Antona, F., Milone, A. P., Tailo, M., et al. 2017, NatAs, 1, 186
Dotter, A. 2016, ApJS, 222, 8
For, B-Q., & Bekki, K. 2017, MNRAS, 468, L11
Georgy, C., Ekström, S., Granada, A., et al. 2013, A&A, 553, A24
Goudfrooij, P., Girardi, L., Kozhurina-Platais, V., et al. 2014, ApJ, 797, 35

Goudfrooij, P., Puzia, T. H., Chandar, R., & Kozhurina-Platais, V. 2011, ApJ, 737, 4
Goudfrooij, P., Puzia, T. H., Kozhurina-Platais, V., & Chandar, R. 2009, AJ, 137, 4988
Gratton, R. G., Carretta, E., & Bragaglia, A. 2012, A&ARv, 20, 50
Hollyhead, K., Bastian, N., Adamo, A., et al. 2015, MNRAS, 449, 1106
Hummel, W. 1994, A&A, 289, 458
Johnson, C. I., McDonald, I., Pilachowski, C. A., et al. 2015, AJ, 149, 71
Keller, S. C., Mackey, A. D., & DaCosta, G. S. 2011, ApJ, 731, 22
Mackey, A. D., & Broby Nielsen, P. 2007, MNRAS, 379, 151
Mackey, A. D., Broby Nielsen, P., Ferguson, A. M. N., & Richardon, J. C. 2008, ApJL, 681, L17
Mateo, M., Bailey, J. I., Crane, J., et al. 2012, Proc. SPIE, 8446, 84464Y
McLaughlin, D. E., & van der Marel, R. P. 2005, ApJS, 161, 304
Milone, A. P., Bedin, L. R., Piotto, G., et al. 2015, MNRAS, 450, 3750
Milone, A. P., Bedin, L. R., Piotto, G., & Anderson, J. 2009, A&A, 497, 755
Milone, A. P., Marino, A. F., D'Antona, F., et al. 2016, MNRAS, 458, 4368
Milone, A. P., Marino, A. F., D'Antona, F., et al. 2017, MNRAS, 465, 4363
Mucciarelli, A., Cristallo, S., Brocato, E., et al. 2011, MNRAS, 413, 837
Niederhofer, F., Bastian, N., Kozhurina-Platais, V., et al. 2016, A&A, 586, A148
Niederhofer, F., Georgy, C., Bastian, N., & Ekström, S. 2015, MNRAS, 453, 2070
Nieva, M. F., & Przybilla, N. 2007, A&A, 467, 295
Paul, K. T., Shruthi, S. B., & Subramaniam, A. 2017, JApA, 38, 6
Piotto, G., Bedin, L. R., Anderson, J., et al. 2007, ApJL, 661, L53
Przybilla, N., & Butler, K. 2004, ApJ, 609, 1181
Reid, W. A., & Parker, Q. A. 2012, MNRAS, 425, 355
Renzini, A., D'Antona, F., Cassisi, S., et al. 2015, MNRAS, 454, 4197
Rivinius, T., Carciofi, A. C., & Martayan, C. 2013, A&ARv, 21, 69
Salinas, R., Pajkos, M. A., Strader, J., Vivas, A. K., & Contreras Ramos, R. 2016, ApJL, 832, L14
Struve, O. 1931, ApJ, 73, 94